Calculated oscillation periods of the interlayer coupling in Fe/Cr/Fe and Fe/Mo/Fe sandwiches

S. Mirbt, A. M. N. Niklasson, and B. Johansson

Condensed Matter Theory Group, Department of Physics, Uppsala University, S-75121 Uppsala, Sweden

H. L. Skriver

Center for Atomic-scale Materials Physics and Department of Physics,
Technical University of Denmark, DK-2800 Lyngby, Denmark
(Received 2 November 1995; revised manuscript received 29 March 1996)

We have performed an *ab initio* study of the oscillation periods of the interlayer coupling in sandwiches of [100] layers of body centered cubic Cr, respectively, Mo, with up to 20 monolayers thickness embedded in an Fe host. Our derived values for the oscillation periods of the interlayer coupling agree well with those expected from the respective Fermi surface calipers and are in excellent agreement with experiment. We compare the interlayer coupling across a nonenhanced paramagnetic Cr spacer with the interlayer coupling across a Cr spacer in the spin-density wave state. We find that the spin-density wave gives rise to an additional contribution to the interlayer coupling. The origin of the observed and calculated 18 Å period of the interlayer coupling can be explained as due to a caliper of the Fermi surface of Cr in the CsCl structure. In the case of the Mo spacer we investigate the influence of the lattice constant on the interlayer coupling and also the dependence of the interlayer coupling amplitude on the Fe magnetic moment. [S0163-1829(96)00633-9]

I. INTRODUCTION

The oscillation of the interlayer coupling as a function of the spacer thickness has been extensively studied in recent years. In 1986 Grünberg *et al.*[1] found an antiferromagnetic interlayer coupling in a (100)-oriented Fe/Cr/Fe sandwich. Later, Parkin *et al.*[2] systematically investigated the interlayer coupling for all transition metals as a spacer imbedded in Co by measuring the giant magnetoresistance. Among these systems, the Fe/Cr/Fe system is a special case for the following two reasons.

First, Cr is an antiferromagnet in contrast to the other investigated spacer materials which are paramagnets. Therefore the question arises of how much the exchange enhancement (see Sec. III A) of Cr influences the interlayer coupling. Up to now all model calculations and all total-energy calculations which make use of the force theorem[3] have neglected the exchange enhancement effects. In order to answer this question we performed two sets of self-consistent total-energy calculations, one where the Cr exchange enhancement was supressed by treating Cr as a paramagnet, and another one where we allowed for the Cr exchange enhancement by letting Cr build up an incommensurable spin-density wave.

Second, experiments have found an extraordinarily long period (18 Å) for Cr as a spacer, despite the fact that the bcc-Cr Fermi surface does not display a corresponding caliper. We show, however, that the CsCl-structure-Cr Fermi surface exhibits exactly the 18 Å caliper, where the CsCl structure is the same as the bcc structure but with two atoms in the unit cell. This observation seems to rule out other possible explanations for the experimentally observed long period oscillation, e.g., that it is not a higher harmonic of the short period oscillation as Schilfgaarde *et al.* suggest,[4] and that it is not due to small variations of the Fermi energy as for example Koelling[5] has suggested.

Since the Fermi surfaces of Mo and Cr are very similar, we have also studied the Fe/Mo/Fe system. It is known[6,7] that Cr has a 2.1 ML oscillation, which is connected with the nesting properties of the Cr Fermi surface. In correspondence to this, for the Mo spacer we also find a 2 ML oscillation, which has already been predicted by Koelling[5] and Levy *et al.*,[8] based on the nesting properties of the Fermi surface. The long period that we find for Mo (15 Å) is in excellent agreement with what is implied by the Fermi surface. However, our calculational method does not take lattice relaxations into account. Since the lattice constants of Fe and Mo differ by about 9%, we made one set of calculations where we used the lattice constant of Mo, a_{Mo}, for the entire sandwich, i.e., for both Fe and Mo, and analogously one set of calculations where we used the lattice constant of Fe, a_{Fe}. This gives us an idea about the influence of lattice relaxations on the interlayer coupling. Moreover, the choice of lattice constant affects the magnitude of the magnetic moment. We calculate that the Fe bulk magnetic moment is $2.23\mu_B$ using a_{Fe} and $2.72\mu_B$ using a_{Mo}. We will show that this difference in the Fe magnetic moment is responsible for the difference in the interlayer coupling amplitudes for the two lattice constants. The organization of the paper is the following. In Sec. II we describe the details of our calculations. In Sec. III we present our results for the Fe/Cr/Fe sandwich, and in Sec. IV we present our results for the Fe/Mo/Fe sandwich. Finally in Sec. V we summarize our results.

II. CALCULATIONAL METHOD

We have performed self-consistent electronic structure calculations by means of the scalar relativistic spin-polarized Green's-function technique[9] based on the linear muffin-tin orbitals method[10] within the tight-binding,[11] frozen core, and atomic-sphere approximations. This has been done using the

local spin-density approximation in the Vosko-Wilk-Nusair parametrization scheme.[12] The Fe/Cr/Fe (Fe/Mo/Fe) sandwiches were constructed by embedding n [100] layers of Cr (Mo) between two semi-infinite body centered cubic crystals of Fe, which symbolically may be written in the form

$$\infty \cdots \text{Fe}\{\text{Cr}\}_n \text{Fe} \cdots \infty. \tag{1}$$

For the Fe/Cr/Fe sandwich the atomic Wigner-Seitz radius is assumed to be 2.662 bohr for both Fe and Cr corresponding to the experimentally observed volume of bcc Fe. The Green's-function technique takes into account the broken symmetry perpendicular to the interface and therefore deals correctly with the purely two-dimensional symmetry of the problem. The interlayer coupling is very sensitive to the topology of the Fermi surface. Therefore it is important to perform the k point and energy integration with high accuracy. We use the principal layer technique[13] and thereby avoid an integration over $k_\perp$, the component of the wave vector perpendicular to the Cr layers. Within our method we have thus no $k_\perp$, but only $k_\parallel$. The direction perpendicular to the Cr layers is dealt with in real space. For the $k_\parallel$ integration we find that 528 special k points[14] in the irreducible part of the two-dimensional Brillouin zone are sufficient for spacer thicknesses up to 20 layers. The energy integration was performed at 16 logarithmically spaced points on a semicircular contour in the complex energy plane. The point on the contour closest to the real axis lies 70 meV below it. This is comparable to a temperature smearing of 235 K. The principal layer consists of three atomic layers which implies that the total number of layers, of Fe and Cr, has to be a multiple of three. Thus the bulk Fe on each side of the sandwich is adjusted in the range 3–5 Fe layers depending on the number of spacer layers.

III. Fe-Cr-Fe

A. Exchange enhancement

The enhanced susceptibilty, $\chi(q)$, of Cr can be written in terms of the Pauli spin susceptibility, $\chi_0(q)$, according to

$$\chi(q) = \frac{\chi_0(q)}{1 - I\chi_0(q)}, \tag{2}$$

where I is the Stoner exchange parameter. If we assume $I=0$, the susceptibilty $\chi(q)$ is equal to the nonenhanced Pauli spin susceptibility $\chi_0(q)$. For nonenhanced paramagnetic Cr, hereafter denoted Cr_PM, we require $\chi(q)=\chi_0(q)$. In our calculation we achieve the restriction $\chi(q)=\chi_0(q)$ in the following way: The exchange-correlation energy in the spin-polarized case is

$$\epsilon_{xc}(r_s, \zeta) = \epsilon_{xc}^\text{PM}(r_s) + \Delta\epsilon_{xc}(r_s, \zeta), \tag{3}$$

where r_s and ζ are the standard variables for density and spin polarization, respectively, and PM stands for paramagnet. During the entire self-consistency cycle we use for Cr_PM

$$\epsilon_{xc}(r_s, \zeta) = \epsilon_{xc}^\text{PM}(r_s), \tag{4}$$

i.e., we only allow those exchange and correlation interactions which are inherent in a paramagnetic system.

TABLE I. Fitting parameters and Fermi-surface calipers of Cr in the CsCl structure.

	Cr_SDW			Cr_PM			Fermi
i	ω_i (ML)	A_i (meV)	Φ_i	ω_i (ML)	A_i (meV)	Φ_i	Q_i (ML)
1	2.05	326	-0.70	2.07	99	-0.31	2.10
2	3.43	431	3.87	2.66	315	-5.53	2.64
3	5.02	910	7.56	3.61	246	-0.65	3.88
4	11.05	738	-0.71	11.98	486	2.82	11.6

We emphasize that this does not imply that the Cr magnetic moment is identical to zero, since a paramagnet under the influence of a magnetic field (in our case the surrounding Fe layers) is indeed spin polarized.

It is well known that Cr at room temperature is an antiferromagnet but in LSDA it is calculated to be a paramagnet[15] at its equilibrium volume. Neither does Cr become antiferromagnetic (AFM) in our calculations in which we allow for the exchange enhancement in Cr, i.e., $I \neq 0$, but it does build up an incommensurable spin-density wave (SDW). The difference between an AFM and the SDW solution becomes particularly evident at large Cr thicknesses. For an AFM solution the magnetic moment of Cr is independent of the layer thickness, whereas for the SDW solution the magnetic moment of Cr decreases with the layer thickness.

B. Interlayer coupling oscillation

We have calculated the total energy for two distinct magnetic configurations where the alignment of the Fe magnetic moments between the two separated Fe sides were either parallel or antiparallel. Hence the interlayer coupling J is defined as the energy difference

$$J(d) = E_\text{tot}^{\uparrow\downarrow}(d) - E_\text{tot}^{\uparrow\uparrow}(d), \tag{5}$$

where d is the spacer thickness and E_tot is the total energy. For small spacer thicknesses the interlayer coupling decreases exponentially and the k points which contribute to the interlayer coupling do not necessarily fulfill the stationary phase condition. Therefore we only include thicknesses larger than 5 ML in the following analysis. To extract the oscillation periods we perform a least squares fit of our calculated interlayer coupling J to the asymptotic limit of the RKKY expression:

$$J = \frac{A_1 \sin(\omega_1 d + \phi_1)}{d} + \sum_{i=2}^{4} \frac{A_i \sin(\omega_i d + \phi_i)}{d^2}. \tag{6}$$

The first term on the right-hand side has a $1/d$ dependence. This is expected for full planar nesting, i.e., for the short period oscillation. The terms in the summation show the usual $1/d^2$ dependence, which is expected for calipers between extrema of the Fermi surface.[16] This expression contains 12 parameters, the fitted values of which are found in Table I. Both configurations, SDW and PM, have been treated separately but we find that the fit for J_{Cr_PM} agrees better with the values of the self-consistent calculation (the root mean square amounts to 0.8 meV for Cr_PM and to 2.2 meV for Cr_SDW). This is also evident in Figs. 1 and 2, where
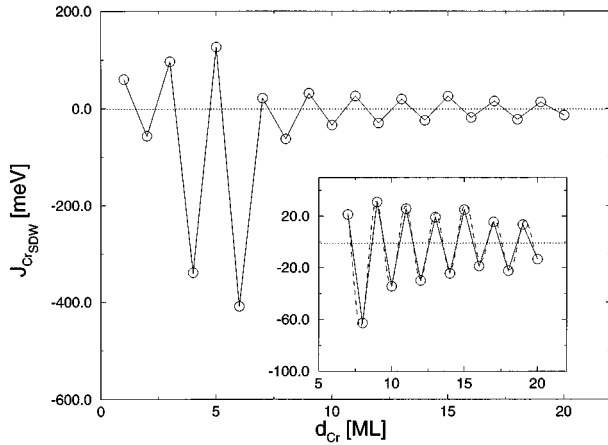
FIG. 1. Calculated interlayer coupling $J_{Cr_{SDW}}$ as a function of the Cr_{SDW} spacer thickness d_{Cr}. The inset shows $J_{Cr_{SDW}}$ (solid line) together with the fit (broken line) in the asymptotic regime.

we show the calculated interlayer coupling together with the fit. Nevertheless, the agreement between the calculated curve and the fit is quite good in both cases. Both for Cr_{PM} and Cr_{SDW} we obtain a short period oscillation (SPO), 2 ML, and a long period oscillation (LPO), 11.5 ML. Both the LPO and the SPO are in excellent agreement with experiment[1,6] as well as with the Fermi surface calipers (Fig. 3 and Table I). However, the experimentally obtained amplitude[1] of the interlayer coupling is about 10^3 times smaller than the calculated amplitude.

From Figs. 1 and 2 we notice two different preasymptotic behaviors. For the 1 ML Cr spacer, the interlayer coupling amplitudes, i.e., $J_{Cr_{PM}}$ and $J_{Cr_{SDW}}$, are more or less identical, whereas between 2 and 6 ML $J_{Cr_{PM}}$ is smaller than $J_{Cr_{SDW}}$ by nearly 2 orders of magnitude. We find that the frustration of the spin-density wave (see Sec. III D) is energetically more expensive in the preasymptotic regime than in the asymptotic regime. This explains the large amplitude of $J_{Cr_{SDW}}$ in the preasymptotic regime.

Besides the SPO and the LPO we find a 2.66 ML and a 3.61 ML period for Cr_{PM}. These two intermediate periods
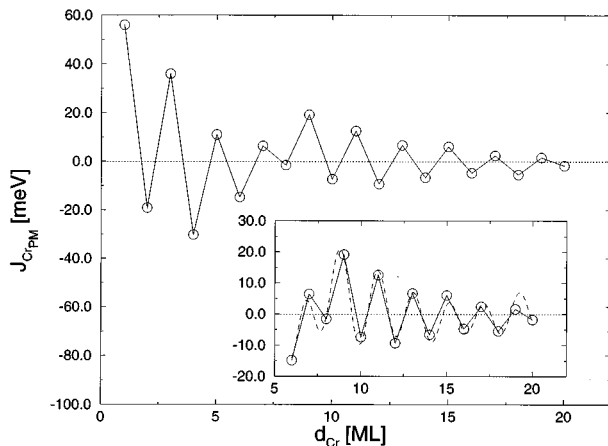

FIG. 2. Calculated interlayer coupling $J_{Cr_{PM}}$ as a function of the Cr_{PM} spacer thickness d_{Cr}. The inset shows $J_{Cr_{PM}}$ (solid line) together with the fit (broken line) in the asymptotic regime.
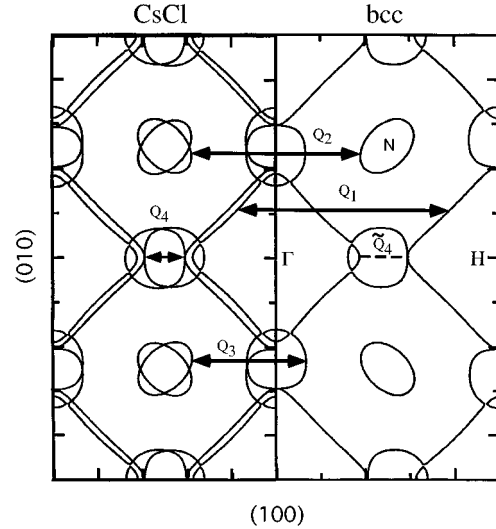

FIG. 3. Fermi surface of bulk Cr along the $\Gamma-H$ direction ($k_\perp$). The lines indicate extremal spanning vectors. We show the Fermi surface in the bcc structure, but in the left half of the figure we also show the Fermi surface in the CsCl structure.

are in very good agreement with the corresponding Fermi surface calipers. This notwithstanding neither the 2.66 nor the 3.61 ML period have been verified experimentally. On the other hand, experiment reveals a 3 ML period for a Mo spacer, which has a Fermi surface very similar to the one of Cr (see Sec. IV A). However, the amplitude of the 2.66 ML period with Cr as a spacer is smaller than the 3 ML period with Mo as a spacer, which might be the reason why it has not been observed yet.

In the case of Cr_{SDW} we find 3.4 ML and 5.0 ML periods. None of these two periods matches with any Fermi surface caliper of Fig. 3, but in Ref. 17 Stiles finds by means of a model calculation a 5.0 ML Fermi surface caliper having its origin in a Fermi surface plane parallel to the one shown in Fig. 3, i.e., $k_\parallel \neq 0$. This concludes the discussion about the intermediate periods and we now turn our attention to the SPO and LPO.

1. Short period oscillation

We find a 2.07 ML, respectively, 2.05 ML, period (Table I) both of which are in excellent agreement with the experimental value of 2.11 ± 0.03 ML (Ref. 6) and the length of the nesting caliper of 2.10 ML (Fig. 3).

Due to the incommensurability of the SPO with the lattice a phase slip occurs with a period of

$$T_{\text{phase slip}} = \frac{T_{SPO}}{|2-T_{SPO}|}. \quad (7)$$

With the calculated SPO (2.07 ML) we get a phase slip every 29 ML, whereas experimentally at room temperature a phase slip is obtained every 22 ML. In our calculation the period of the phase slip is governed by the difference between the kinetic energy and the sum of Hartree and exchange-correlation energy. Thus the behavior of the phase slip strongly depends on the calculational accuracy of the total energy. If we fix the E_ν parameter[10] at its bulk value, we
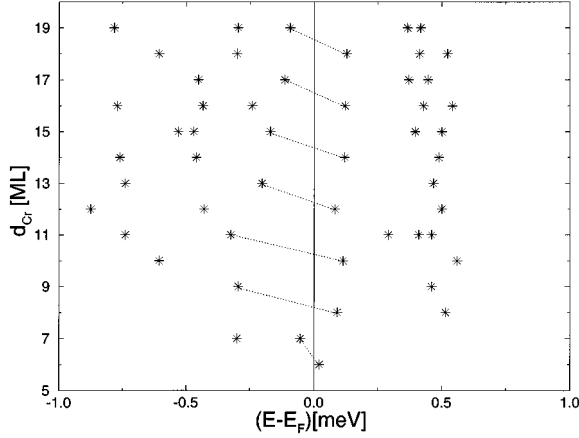
FIG. 4. Dispersion of QW states with thickness. The energy position of the QW states relative to the Fermi energy as a function of the Cr thickness is shown for one nesting k point $k_\parallel = (0,0.25)$ when the Fe magnetic moments aligned parallel. The broken lines indicate the periodic movement of the QW peaks through the Fermi energy.

FIG. 5. Energy position of the QW states for $d_{Cr} = 16$ ML and the nesting k point $k_\parallel = (0,0.25)$ when the Fe magnetic moments are aligned parallel. For this thickness the SDW is frustrated. The solid (dotted) line indicates the QW states of Cr_{SDW} (Cr_{PM}) and for comparison the dashed line shows the QW states of Mo (a_{Mo}) in the Fe/Mo/Fe system, i.e., a system for which the SPO follows the strong scattering limit.

obtain a phase slip at 13–14 ML in agreement with the calculation by Schilfgaarde $et\ al.$[18] If we include the E_ν parameter in the self-consistent procedure, i.e., if we always choose E_ν at the center of the occupied density of states, we expect a phase slip at about 29 ML. Unfortunately, the calculated interlayer coupling for $d_{Cr} > 20$ ML was not fully converged within the computational limits. Moreover, the phase slip depends on the accuracy of the calculated short period oscillation (SPO). Let us assume a value of 2.07 ± 0.02 ML. With this accuracy the phase slip can vary between 23 ML and 41 ML, which shows the difficulty to compare the calculated result of the phase slip with experiment.

For a discussion of the amplitude of the SPO, we caculate the spectral density D_s,

$$ D_s(E, \mathbf{k}_\parallel) = -\frac{1}{\pi} \mathrm{Im}\, \mathrm{Tr} \sum_i\ G_{ii}(E, \mathbf{k}_\parallel), \qquad (8) $$

for $\mathbf{k}_\parallel$ equal to a nesting point. The trace is to be taken over the orbitals and G_{ii} is the Green's function of the layer i. We do not include all layers i in the above summation because otherwise the existing interface states would complicate the interpretation of the spectral density peaks. Every peak in the spectral density that moves periodically through the Fermi energy with increasing spacer thickness corresponds to a quantum well (QW) state. In Fig. 4 we show the dispersion of the QW states for the nesting calipers, i.e., the energy position of the QW state for different spacer thicknesses. The stars in the figure correspond to peaks in the spectral density and the lines indicate the periodical movement of the QW states through the Fermi energy. The period of the QW states amounts to 2.07 ± 0.02 ML which is in excellent agreement with the fitted SPO and the nesting caliper. In Fig. 5 we display the energy dependence of the QW states for a particular spacer thickness. The QW states are rather broad compared to Mo, for example. A look at the band structure along $k_\perp$ at that nesting point (Fig. 6) for both Fe and Cr reveals that the Cr wave functions at the Fermi energy do not experience an energy gap. This is not the case for all nesting
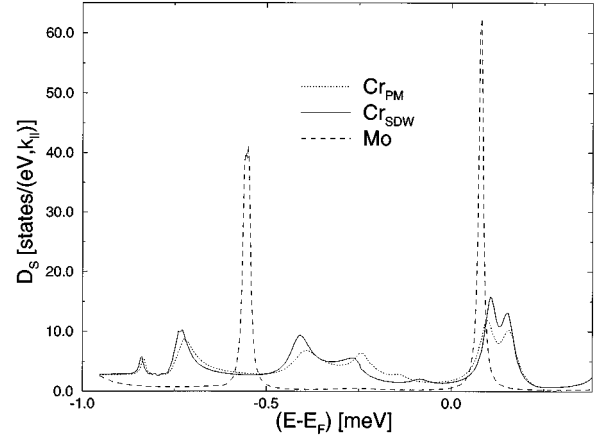
points, since in the range of $(0,0) < \mathbf{k}_\parallel < (0,0.25)$, the Cr wave functions indeed experience a gap.

2. Long period oscillation

As already pointed out in the Introduction, the nature of the LPO in Cr has been puzzling for quite a long time. Until now, no first-principles calculation could reproduce the LPO. Moreover, the fact that the bcc Cr Fermi surface offers no caliper of a length that would correspond to the LPO left room for speculations. Recently, Schilfgaarde and Harrison[4] argued that the LPO might be a higher harmonic of the SPO. Their argumentation seems to lead to the conclusion that the phase slip period is identical to the period of the long oscillation, which certainly is not true.[1,6] Koelling $et\ al.$ suggested that a small change in the Fermi energy might modify the topology of the bcc Fermi surface such that the 9 ML caliper changes to a $10-12$ ML caliper. We investigated the bcc Fermi surface for a different value of the Fermi energy $[E_F(T=0) + T = 300\ \mathrm{K}]$ and found no changes that would give rise to a $10-12$ ML caliper.

In the past, the bcc Cr Fermi surface has been investigated in order to find the caliper which gives rise to the LPO. Investigating instead the Fermi surface of Cr in the CsCl structure, i.e., that the unit cell of the Cr consists of two atoms per cell, we found that the Cr Fermi surface in the CsCl structure gives rise to different calipers than in the bcc structure as long as the nesting caliper is incommensurable with the lattice. In the bcc structure a caliper Q along the (100) direction, fulfills the following equation:

$$ Q + k = G_{bcc}, \qquad (9) $$

where G_{bcc} is the reciprocal lattice vector of the bcc lattice. In the CsCl structure the same caliper Q fulfills instead the following equation:
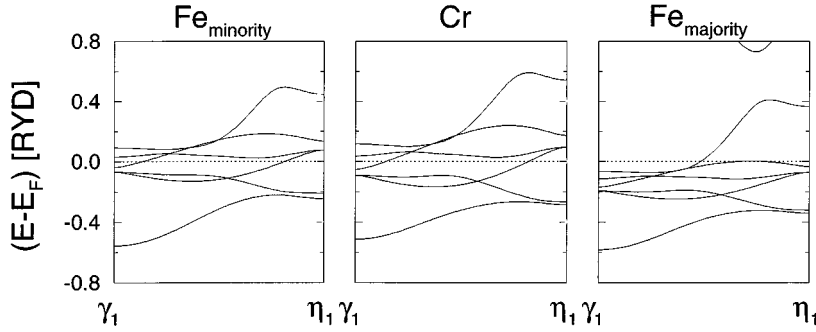
FIG. 6. Energy bands along a nesting caliper in Fe and Cr. The left panel shows the Fe spin-down bands and the right panel the Fe spin-up bands. The middle panel shows the Cr bands. η_1 has the coordinates, $(2\pi/a)(0,0.25,0)$ and γ_1 the coordinates $(2\pi/a)(0,0.25,1)$.

$$Q+k' = \frac{G_{\text{bcc}}}{2}. \qquad (10)$$

If we now assume the caliper spanning the hole octahedron at H in the bcc structure to be identical with Q in Eq. (9) and Eq. (10), the caliper Q_4 in Fig. 3 is identical to k' in Eq. (10). As long as the nesting caliper Q_1 is incommensurable with the lattice, we find no caliper in the bcc structure which is identical with Q_4 in Fig. 3. In other words, the calipers Q_4 and $\widetilde{Q}_4$ have different lengths as long as Q_1 is incommensurable with the lattice.

If paramagnetic Cr is correctly described assuming a bcc structure, the bcc and CsCl Fermi surfaces should give rise to the same calipers. Our findings suggest that even our paramagnetic bulk solution is not correctly describable assuming a bcc structure for Cr, i.e., the CsCl structure of Cr is not reducible to a bcc structure, as long as the nesting caliper of Cr is incommensurable with the lattice. In agreement with our findings Schwartzman et al.[19] showed that if many-particle effects, i.e., exchange and correlation, are neglected, the susceptibility of paramagnetic Cr has a sharp peak near the nesting caliper in contrast to Mo.

Since Cr has an incommensurable nesting vector the CsCl and bcc Cr Fermi surface give rise to different calipers at the Γ point, i.e., the calipers Q_4 and $\widetilde{Q}_4$ give rise to different periods. Calipers $Q_1, Q_2,$ and Q_3 are identical for the bcc and CsCl-Cr Fermi surface. For the CsCl Fermi surface the Q_4 caliper is 11.6 ML long and gives rise to an intraband transition, whereas for the bcc Cr Fermi surface the $\widetilde{Q}_4$ caliper is 9.3 ML long and gives rise to an interband transition which exactly at the Γ point even is symmetry forbidden (Fig. 3). This means that the agreement is excellent between the Fermi-surface calipers, the fitted interlayer coupling periods, and the experimentally obtained interlayer coupling periods if we use the paramagnetic CsCl Fermi surface.

In the case of, say, bcc Cu the calipers of the CsCl and of the bcc Fermi surface are exactly the same because there is no incommensurable nesting vector. The correct description of Cr is a unit cell which contains two atoms per cell. By increasing the number of atoms per unit cell even more, for example, by using four atoms, the lengths of the calipers do not change.

C. Contributions to the interlayer coupling

In this section we describe the interlayer coupling for Cr_{SDW} by considering it as a sum of two distinct contribu-

tions, namely, the spin-density wave contribution J_{SDW} and the multiple scattering contribution $J_{scattering}$,

$$J_{Cr_{SDW}} = J_{SDW} + J_{scattering}. \qquad (11)$$

For Cr as a paramagnetic spacer the interlayer coupling has its origin merely in multiple scattering. Therefore the multiple scattering contribution to the interlayer coupling across the Cr_{SDW} spacer approximately equals the total interlayer coupling across the paramagnetic Cr spacer, $J_{scattering} = J_{Cr_{PM}}$.

For a spacer thickness where the SDW in Cr is frustrated, Fig. 5 displays the spectral density for one nesting point for both the Cr_{PM} and the Cr_{SDW} spacer and confirms the above equality. For spacer thicknesses where the SDW in Cr is frustrated (Sec. III D) there exists nearly no SDW contribution to the spectral density. Therefore the spectral densities for Cr_{PM} and Cr_{SDW} in Fig. 5 should be rather similar to each other. The small differences in the spectral densities have their origin in slightly different boundary conditions at the Fe interface. (Due to hybridization the Fe interface moment depends on whether it is in contact with a Cr_{PM} spacer or a Cr_{SDW} spacer.) In Fig. 7 we show, as in Fig. 5, the spectral density for one nesting point for both the Cr_{PM} and the Cr_{SDW} spacer, but now for a spacer thickness where the SDW in Cr is matched at the Fe interface. We notice that the spectral density peaks of Cr_{SDW} are exchange shifted and
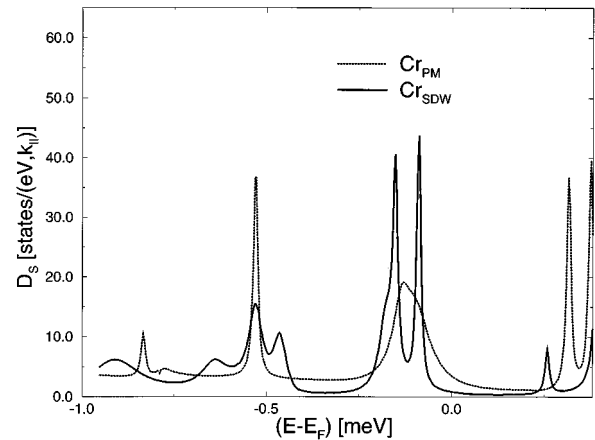

FIG. 7. Energy position of the QW states for $d_{Cr} = 15$ ML and the nesting k point $k_{\parallel} = (0,0.25)$ when the Fe magnetic moments are aligned parallel. This thickness allows the formation of a SDW. The solid (dotted) line indicates the QW states of Cr_{SDW} (Cr_{PM}).
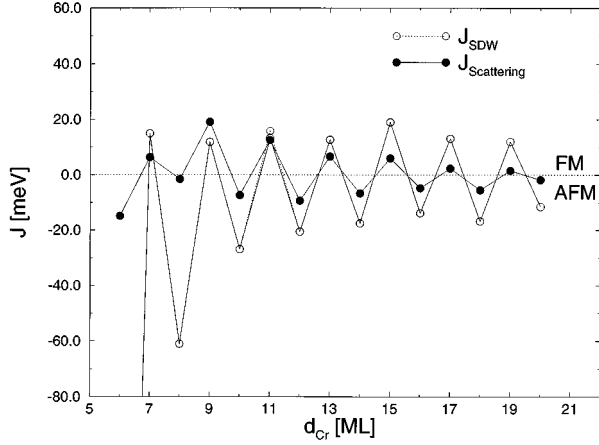
FIG. 8. The multiple-scattering contribution $J_{\text{scattering}}$ and the spin-density wave contribution J_{SDW} as a function of the spacer thickness d_{Cr}.

amplified compared to the peaks of Cr_{PM}. For all Cr layers having a positive (negative) magnetic moment the peaks are shifted by plus (minus) half the exchange splitting compared to the peaks of Cr_{PM}.

Now we can compare the two different contributions to the interlayer coupling, i.e., $J_{\text{SDW}} = J_{\text{Cr}_{\text{SDW}}} - J_{\text{Cr}_{\text{PM}}}$ since $J_{\text{scattering}} = J_{\text{Cr}_{\text{PM}}}$. In Fig. 8 we show both the spin-density wave and the multiple scattering contribution to the interlayer coupling across the Cr_{SDW} spacer. We notice that both contributions are of the same order of magnitude. Therefore the interlayer coupling for a Cr spacer has two equally important contributions, multiple scattering[16] and spin-density wave. The effect of the spin-density wave in Cr is to force the magnetic moments of the ferromagnetic layer to align with the magnetic moment of the closest Cr layer. For most spacer materials the spin-density wave contribution is negligible, as in Mo, or even absent, as in Cu. In most cases the multiple scattering contribution is equal to the interlayer coupling, i.e., $J = J_{\text{MS}}$. For Cr, on the other hand, there exists in addition a spin-density wave contribution, since Fe induces a spin-density wave in Cr. We expect an antiferromagnetic calculation to give about the same results for J_{SDW} as obtained here, since for the presently investigated range of spacer thicknesses the amplitude of the SDW in Cr is more or less constant within the spacer (see Sec. III D).

D. Magnetic properties

In Fig. 9 we compare the magnetic moment profiles for Cr_{SDW} with Cr_{PM}. For an odd (even) number of spacer layers the absolute value of the magnitude of the Cr magnetic moment has to go through zero, if the Fe magnetic moments are aligned antiparallel (parallel).[7] In short, this behavior is due to the boundary conditions the spin-density wave experiences at the interface, i.e., we have one situation where the spin-density wave is matched at the Fe interface and another situation where the spin-density wave is frustrated. In the matched situation (left graph) the Cr interface magnetic moment for Cr_{PM} is reduced to 26% and in the following layer it is reduced even further to 6% compared to the respective moments of Cr_{SDW}. We point out that the magnetic moment
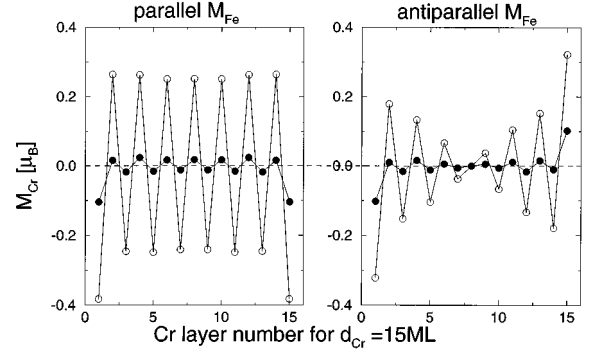

FIG. 9. Magnetic moment of Cr_{SDW} and Cr_{PM} for a parallel alignment (left graph) and an antiparallel alignment (right graph) of the Fe moments for $d_{\text{Cr}} = 15$ ML.

of Cr_{SDW} decreases only slightly with layer thickness as is evident from Fig. 9 (left). At the interface the Fe magnetic moment is reduced due to hybridization with Cr.[20] At the interface with Cr_{SDW} (Cr_{PM}) the Fe moment amounts to $1.97\mu_B$ ($1.91\mu_B$), which corresponds to a 14% reduction compared to the magnetic moment of bulk Fe.

IV. Fe/Mo/Fe

A. Fermi surface

The oscillation periods of the interlayer coupling J are determined by the Fermi-surface topology. In the asymptotic limit, i.e., for large distances d between the Fe layers, the RKKY theory predicts $J \sim e^{i2\vec{k}_F\vec{d}}$ in the free-electron case[21] and $J \sim e^{i(\vec{k}_i - \vec{k}_j)\vec{d}}$ for a periodic potential, where $\vec{d}$ points in the direction perpendicular to the interfaces. Thus it is the difference between two k points at the Fermi energy, $\vec{k}_i - \vec{k}_j$, that determines the periods of the interlayer coupling. The vectors $\vec{k}_i$ and $\vec{k}_j$ have to fulfill the following four conditions in order to asymptotically determine the periods of the interlayer coupling: First $\vec{k}_i$ and $\vec{k}_j$ have to lie on the Fermi surface, second $(\vec{k}_i - \vec{k}_j) \| \vec{d}$, third the group velocities $\vec{v}_i$ and $\vec{v}_j$ must be antiparallel, and fourth the band symmetry in points $\vec{k}_i$ and $\vec{k}_j$ must be the same.

In Fig. 10 we show the Fermi surface of bulk-Mo with the experimental lattice constant of Mo, $a_{\text{Mo}} = 3.14$ Å, and with the experimental lattice constant of Fe, $a_{\text{Fe}} = 2.86$ Å. Some pairs of **k** points (calipers), which fulfill the above-mentioned conditions and therefore contribute to the oscillation of the interlayer coupling in the asymptotic limit are indicated by arrows: Caliper Q_1 is the nesting caliper. It connects the jack centered on Γ with the octahedron centered on H (2 ML). Caliper Q_2 connects the ellipses at N. The caliper Q_3 connects the ellipse at N with the jack. Finally, the caliper Q_4 connects the jack with the lens found along the Δ line from Γ to H. The lengths of the calipers depend on the value chosen for the Mo lattice constant. The 2 ML caliper is shorter using a_{Fe}, whereas the three other calipers are longer using a_{Fe}. The calipers for the two lattice constants which were determined graphically, are collected in
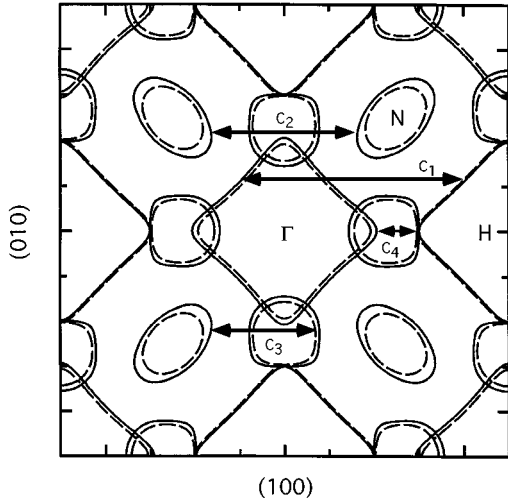
FIG. 10. Fermi surface of bulk Mo along the Γ-H direction ($k_\perp$). The solid (broken) line is the Fermi surface of bulk Mo for the lattice constant a_{Fe} (a_{Mo}). The arrows indicate calipers contributing to the interlayer coupling (see text).

Table II, using the relation $\omega_i = 1/\Lambda_{k_i}$, where ω is the period, Λ_k is the length of the caliper and i labels the four above-mentioned calipers.

TABLE II. Fermi surface calipers of Mo.

ω_i [ML]	a_{Fe}	a_{Mo}
ω_1	2.00	2.05
ω_2	3.11	2.74
ω_3	4.21	4.00
ω_4	10.77	9.66

B. Band structure

The amplitude of the interlayer coupling is determined by the degree of matching between the Fe and Mo bands.[22] The amplitude is small in case the Mo states at the Fermi energy can couple to Fe states, i.e., if there is no gap. The amplitude is larger in case the Mo states at the Fermi energy find no Fe states to couple with, i.e., if there is a gap. In the following we want to investigate the band structure along the four calipers, i.e., along $k_\perp$ for four different $\mathbf{k}_\parallel$. As mentioned above, we have no $\mathbf{k}_\perp$ in our calculation, which implies that it is not obvious which band structure to investigate. We find that the interface-Fe properties, and not the Fe bulk properties, determine the amplitude of the interlayer coupling. Therefore we show the bulk Fe band structure but with the potential parameters[10] of the Fe interface layer. In other words we fix the Fe bulk magnetic moment at the calculated interface magnetic moment. In Figs. 11, 12 and 13 we show the band structures for each caliper, Q_1–Q_4, separately. The bands in the figures are numbered in order of increasing energy at the right zone boundary.

In Fig. 11 we show the bands along the caliper Q_1 for a_{Mo}. For a_{Fe} (not shown, but similar to Fig. 6), the Mo and Fe bands (bands 3 and 5 in Fig. 11) match each other for both spin directions, but for a_{Mo}, only the spin-down bands of Mo and Fe match. The spin-up bands of Fe and Mo are of different symmetry at the Fermi energy, which leads to a gap for the spin-up states of Mo. Thus, for Q_1 we find a gap using a_{Mo}, but no gap using a_{Fe}.

In Fig. 12 we show the bands along Q_2 and Q_3 for a_{Fe}. Calipers Q_2 and Q_3 have about the same $\mathbf{k}_\parallel$, which implies that the band structures along Q_2 to Q_3 do not differ significantly. The bands 2 and 4 give rise to caliper Q_3 whereas caliper Q_2 involves only band 2. For both lattice constants and both calipers the Mo states find Fe states to couple with at the Fermi energy regardless of the spin direction, since the Fe and Mo bands have the same symmetry. We find no gap for either lattice constant and the Fe and Mo bands match.

In Fig. 13 we show the bands along Q_4 for a_{Mo}. The caliper Q_4 connects bands 3 and 4. At first sight it seems as if this caliper violates the symmetry condition. The caliper joins the $\Delta_{2'}$ band (band 4) with the Δ_5 band (band 3). However, we recall that not only the critical point, but a small region around it, contributes to the interlayer coupling. At the Γ point the Δ_5 band is doubly degenerate. But already in a small region around the Γ point this degeneracy is lifted[23] so that the transition between bands 3 and 4 does not violate the symmetry condition. Hence caliper Q_4 fulfills all conditions (Sec. IV A) and thus contributes to the interlayer coupling. For both lattice constants, only the spin-down bands of Fe and Mo match each other, whereas the spin-up Mo states experience a gap. For caliper Q_4 we find gaps using either lattice constant.

C. Interlayer coupling oscillation

We again calculated the total energy for two magnetic configurations, where the Fe magnetic moments either point parallel or antiparallel to each other. Then the interlayer coupling J is defined as in Eq. (5). In Figs. 14 and 15 we show
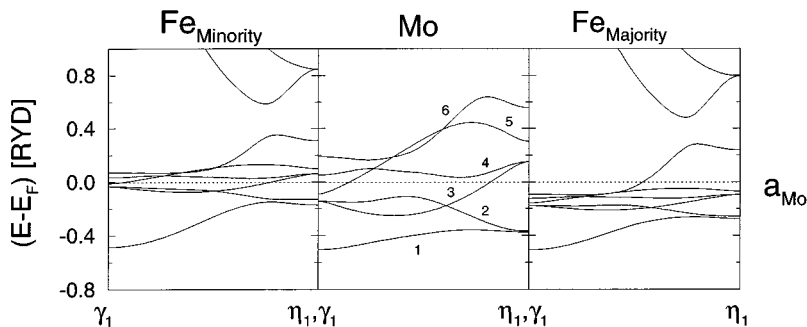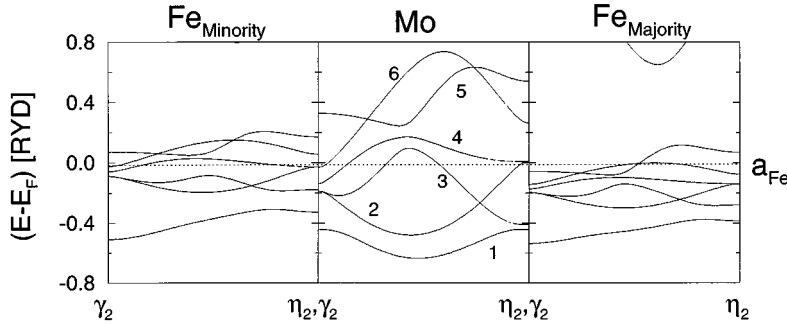

FIG. 11. Energy bands along Q_1 in Fe and Mo for a_{Mo}. The first panel shows the Fe spin-down bands and the last panel the Fe spin-up bands. The panel in between shows the Mo bands. η_1 has the coordinates $(2\pi/a)(0,0.25,0)$ and γ_1 the coordinates $(2\pi/a)(0,0.25,1)$.

FIG. 12. Energy bands along Q_2 (and Q_3) in Fe and Mo for a_{Fe}. The first panel shows the Fe spin-down bands and the last panel the Fe spin-up bands. The panel in between shows the Mo bands. η_2, γ_2, η_3, and γ_3 have the coordinates $(2\pi/a)(0,0.42,0)$, $(2\pi/a)(0,0.42,1)$, $(2\pi/a)(0,0.44,1)$, and $(2\pi/a)(0,0.44,1)$, respectively.

the calculated interlayer coupling J as a function of the spacer thickness d ($d = 1,\ldots,20$ ML) (solid curve). To extract the oscillation periods we again perform a least squares fit of our calculated interlayer coupling J to the asymptotic limit of the RKKY (QW) expression as in Eq. (6). The fit expression contains 12 parameters, the fitted values of which are found in Table III. In order to compare the oscillation periods for the two different values of the lattice constant, we have to do a fit with at least four periods. A fit with only three periods leads to the three strongest periods for the respective a: ω_1, ω_3, and ω_4 for a_{Fe} and ω_1, ω_2, and ω_3 for a_{Mo}. Previously[24] we reported results using only three fit periods all of which have a $1/d$ dependence and did not obtain the 3 ML period for either a.

In the following we compare our fitted periods with the Fermi-surface calipers (Table II). When we compare the second columns of Table II and Table III and the third column of Table II with the fourth column of Table III, we find a nearly perfect agreement. The difference between the Fermi-surface values and the fit values is at most 4% and indicates the exactness and convergence of our computational method. Levy et al.[8] find by use of the Anderson model, only the 2 ML oscillation and others[17,5] find by investigating the possible Kohn-anomaly spanning vectors an extensive list of possible oscillation periods, including the periods found by our fit. Experimentally only the 3 ML oscillation has been found in the (100) direction.[25] Their reported coupling strength amounts to 0.12 meV at $d \approx 5$ ML, which is equivalent to a coupling amplitude $A_2 \approx 3$ meV. Thus the experimentally obtained coupling amplitude is by about a factor of 10^2 smaller than the theoretical one. This is not so surprising, since in our calculation we include neither surface roughness nor defects which both broaden the scattering state and thereby decrease the coupling amplitude. The question of why the other periods have not been observed experimen-

tally is still open. In Ref. 5 Koelling made the argument that the 3 ML oscillation is of sp nature in contrast to the other periods which all contain d character. Then, by defect scattering the d character is washed out, whereas the sp character is less influenced by such factors. This line of argumentation should also be valid for the 4 ML oscillation, which is dominantly of sp character as well. But the 4 ML oscillation is not found experimentally in spite of the fact that theoretically the amplitude of the 4 ML oscillation is even larger than the 3 ML oscillation.

D. Interlayer coupling amplitude

From the theoretical point of view the RKKY (Ref. 16) and the quantum well (QW) theory[22] were both put forward to explain the salient features of the interlayer coupling. There is general agreement that RKKY theory and QW theory are equivalent and that they are capable to explain the features of the interlayer coupling. Both describe a multiple scattering process. If one only considers the lowest contributing scattering order, i.e., one single scattering of the wave function both at the left and right interface, one recovers the RKKY expression found by perturbation theory.[16] This defines the weak scattering limit, which implies that the interlayer coupling amplitude, A, is proportional to the square of the ferromagnet's magnetic moment, M^2.[4,16] If higher orders of scattering are included, i.e., multiple scattering at both interfaces one recovers the QW theory. Higher orders of scattering become important when a gap opens up at the Fermi energy. Then, in the strong scattering limit, the interlayer coupling amplitude is independent of the magnetic moment.[26]

In the following we investigate the dependence of the interlayer coupling amplitude on the magnetic moment of Fe. Earlier Schilfgaarde et al.[4] made a similar investigation for a
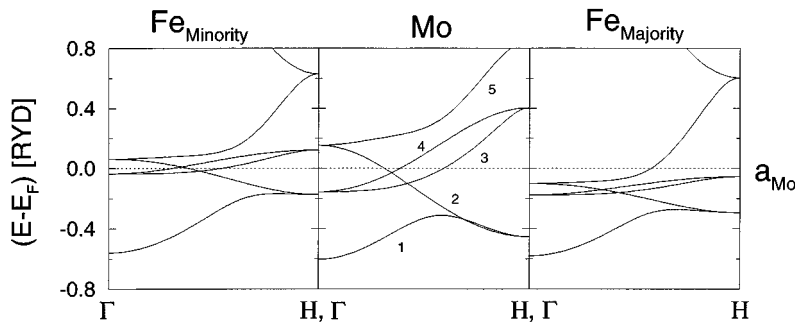

FIG. 13. Energy bands along Q_4 in Fe and Mo for a_{Mo}. The first panel shows the Fe spin-down bands and the last panel the Fe spin-up bands. The panel in between shows the Mo bands.
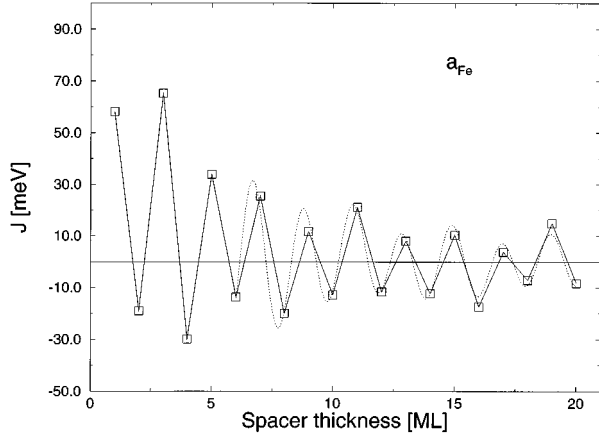
FIG. 14. Calculated interlayer coupling J for a_{Fe} as a function of the Mo spacer thickness. The solid curve gives the self-consistent results and the broken line is the result of the fitting procedure [Eq. (5)].

Fe/Cr/Fe system. In the weak scattering limit, the interlayer coupling amplitude, A, can simply be expressed as a function of the Fermi surface curvature, κ, and the square of the ferromagnet's magnetic moment, M^2.[27] Thus the interlayer coupling does not explicitly depend on the chosen a. Moreover, the Fermi surface curvatures for the two lattice constants differ so little that we may approximate the ratio of the interlayer coupling amplitude by the ratio of the square of the Fe magnetic moments,

$$\frac{A_{a_{Mo}}}{A_{a_{Fe}}} = \frac{M^2_{a_{Mo}}}{M^2_{a_{Fe}}}. \quad (12)$$

The small difference between the Fermi surface curvatures of the two lattice constants is reflected by the difference in the phases obtained by our fit (Table III). For the 2 ML oscillation the difference vanishes. In this case the Fermi surface
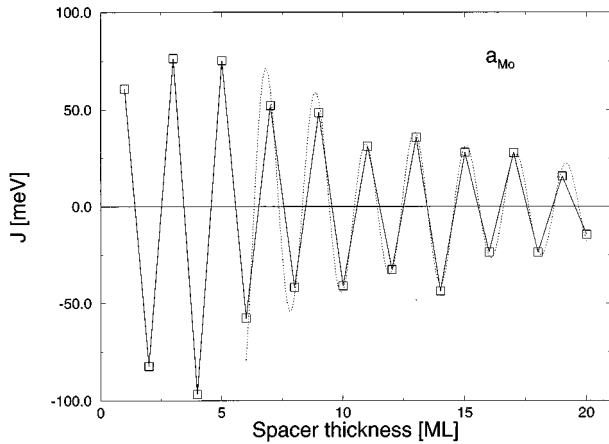

FIG. 15. Calculated interlayer coupling J for a_{Mo} as a function of the Mo spacer thickness. The solid curve gives the self-consistent results and the broken line is the result of the fitting procedure [Eq. (5)].

TABLE III. Fit parameters for the Mo spacer.

		a_{Fe}			a_{Mo}	
i	ω_i (ML)	A_i (meV)	Φ_i	ω_i (ML)	A_i (meV)	Φ_i
1	2.04	181	-0.32	2.06	462	-0.30
2	3.09	287	2.49	2.78	644	-1.45
3	4.03	495	3.66	3.94	699	0.66
4	11.2	355	2.02	9.66	226	2.59

curvatures are equal for both lattice constants (Fig. 10). The difference in the center of band, C, between spin up and spin down,

$$C^\uparrow - C^\downarrow = \Delta C, \quad (13)$$

is to first-order approximation proportional to the difference in occupation numbers between spin up and spin down, i.e., the magnetic moment

$$\Delta C \sim M. \quad (14)$$

From Eqs. (12) and (14) it follows that the amplitude ratio is equal to the ratio of the square of the center of band differences, i.e.,

$$\frac{A_{a_{Mo}}}{A_{a_{Fe}}} = \frac{(\Delta C_{a_{Mo}})^2}{(\Delta C_{a_{Fe}})^2}. \quad (15)$$

In the following we discuss whether Eq. (15) is fulfilled for the four different calipers. In Table IV we compare our fitted amplitudes with the square of the center of band difference. We obtained ΔC graphically by using the Fe bands that give the strongest contribution to the interlayer coupling. Obviously these are bands 3 and 5 for caliper Q_1, band 2 for Q_2, bands 2 and 4 for Q_3, and bands 3 and 4 for Q_4. In the first column we show the amplitude ratio and in the second column we show the ratio of the square of the center of bands difference. For the 3,4, and 10 ML oscillation the two ratios are about equal, i.e., Eq. (15) is fulfilled and thus the amplitude is proportional to the magnetic moment squared. However, for the 2 ML oscillation the two ratios deviate by about 40%, i.e., Eq. (15) is not fulfilled. The band structure at Q_1 along $k_\perp$ tells us that for the a_{Mo} there is a gap contributing to the interlayer coupling, whereas for the a_{Fe} there is not. The disagreement for the 2 ML oscillation is thus expected, since, as mentioned earlier, the appearance of a gap (for the a_{Mo}) implies that the interlayer coupling amplitude is independent on the Fe magnetic moment. In contradiction with theoretical predictions[26] stands that despite the fact that for caliper Q_4 we find a gap for both lattice constants, we find the interlayer coupling amplitude to be pro-

TABLE IV. Comparison between the amplitude ratio and the center of band ratio.

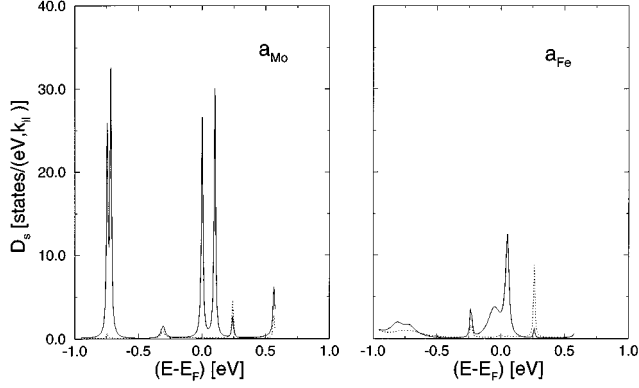| Caliper	$A_{a_{Mo}}/A_{a_{Fe}}$	$\Delta C^2_{a_{Mo}}/\Delta C^2_{a_{Fe}}$
1 (2 ML)	2.6	1.6
2 (3 ML)	2.2	2.5
3 (4 ML)	1.4	1.6
4 (10 ML)	0.6	0.5

FIG. 16. The spectral density [Eq. (8)] for $\mathbf{k}_{\parallel} = (2\pi/a)(0,0.25)$. The left (right) panel gives the spectral density for a_{Mo} (a_{Fe}). The solid line gives the spectral density for i only running over the Mo layers, whereas the broken line gives the spectral density for i equal to the one Fe layer 3 ML away from the interface with Mo.
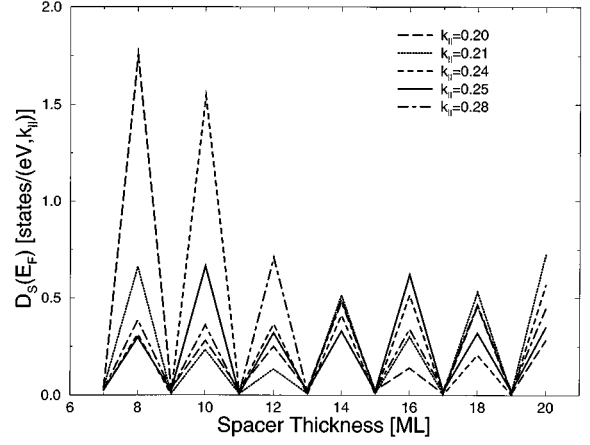

FIG. 17. The spectral density [Eq. (8)] at the Fermi energy as a function of the Mo spacer thickness for $\mathbf{k}_{\parallel} = (2\pi/a)(0,0.25)$ for a_{Fe}. The different lines give the spectral density for different $k_{\parallel}$ points, all of which give rise to a nesting caliper.

portional to the magnetic moment squared. This we cannot explain yet. We have thus shown that the 2 ML oscillation for the a_{Mo} follows the strong scattering limit, whereas the 2 ML oscillation for the a_{Fe} follows the weak scattering limit. The 3 and 4 ML oscillations both follow the weak scattering limit for both lattice constants. For caliper Q_4 we have contradictory results, i.e., from the band structure we would argue that the long period oscillations follows the strong scattering limit but we find it in this section to follow the weak scattering limit.

E. Spectral density

The spectral density D_s [Eq. (8)] can be used to derive some information about the nature of the coupling. The uncertainty relation $\Delta t \Delta E \approx \hbar$ implies that the longer the path of the wave (and thus the larger the time t) is, the smaller will the uncertainty in energy become. The higher the scattering orders that contribute to the interlayer coupling, i.e., the longer the path of the wave function, the narrower becomes the spectral density peak. In the following we will only consider the spin-up states, because the contribution to the interlayer coupling from the spin-down states is much smaller. We calculated the spectral density for one nesting k point $[\mathbf{k}_{\parallel} = (0,0.25)]$ as a function of the energy for the two different lattice constants (Fig. 16). The solid curve corresponds to the Mo spectral density, i.e., i runs over the entire spacer with the exception of the interface layers, whereas the broken curve indicates the Fe spectral density for the one Fe layer furthest away from the interface. For both lattice constants we see at the Fermi energy two peaks which have no counterpart in Fe. These are scattering states. The peak width for the a_{Fe} is considerably broader compared to the peak width for the a_{Mo}, i.e., for a_{Fe} the 2 ML oscillation follows the weak scattering limit while for a_{Mo} already higher scattering orders contribute.

In Fig. 17 we again show the spectral density but this time for a fixed energy, the Fermi energy, and instead as a function of the spacer thickness. The different curves correspond to different k points all contributing to the nesting caliper.

This demonstrates clearly the 2 ML oscillation. Moreover, all nesting k points contribute to the interlayer coupling in a constructive manner. For a Mo thickness of 8 ML the k point with $k_{\parallel} = 0.20$ gives the strongest contribution, whereas for a Mo thickness of 16 ML the same k point gives the weakest contribution. This difference is due to how close to the Fermi energy the scattering peak appears for a particular Mo thickness and k point.

F. Magnetic moment of Fe and Mo

At the Fe/Mo interface, Fe induces a spin polarization in Mo. By considering a single interface, ∞Fe/Mo ∞, one finds that Fe gives rise to a Friedel oscillation in Mo, i.e., the Mo magnetic moment will oscillate in space. In Table V we show the charge and magnetic moment at the Fe/Mo interface. The magnetic moment of Fe is, compared to the bulk, reduced at the interface by 24% for the a_{Fe} and by 20% for the a_{Mo}. This reduction is due to hybridization between the Mo d band and the Fe d band.[20] We find a fast decaying Fe charge oscillation and a slower decaying oscillation of the Fe magnetic moment. Mo behaves as an antiferromagnet with a small magnetic moment. At the interface Mo has a moment of $0.23\mu_B$ for a_{Mo} and of $0.04\mu_B$ for a_{Fe}. At the interface, the Mo and Fe moments always couple antiparallel to each other.

V. SUMMARY

In the case of the Cr spacer we have shown that the magnetic moment of Cr influences the interlayer coupling dra-

TABLE V. Magnetic moment and charge at the Fe/Mo interface.

		Fe	Fe	Fe	Mo	Mo	Mo	Mo	Mo	Mo
a_{Fe}	Q	7.99	7.98	8.35	5.65	6.02	6.00	6.00	6.00	6.00
	M	2.34	2.49	1.68	-0.04	0.01	-0.01	0.02	-0.01	0.01
a_{Mo}	Q	8.00	7.98	8.30	5.70	6.01	6.00	6.00	6.00	6.00
	M	2.72	2.76	2.20	-0.23	0.03	-0.03	0.04	-0.03	0.02

matically. Besides the multiple scattering contribution we find a spin-density wave contribution to the interlayer coupling which is of the same order of magnitude. The 18 Å period of the interlayer coupling can be explained as due to a caliper of the Cr Fermi surface in the CsCl structure. In the case of the Mo spacer we have discussed the Fermi surface of Mo and the band structure of Fe and Mo for four different calipers. We fit four periods to our calculated interlayer coupling and find them in excellent agreement with the Mo Fermi surface calipers. We even find the experimentally observed 3 ML period. With the exception of the 2 ML period

coupling, all the other interlayer coupling amplitudes are proportional to the square of the magnetic moment, despite the fact that for the longest period there exists a gap.

[1] P. Grünberg, R. Schreiber, Y. Pang, M. B. Brodsky, and H. Sowers, Phys. Rev. Lett. **57**, 2442 (1986).
[2] S. S. P. Parkin *et al.*, Phys. Rev. Lett. **64**, 2304 (1990).
[3] A. R. Mackintosh and O. K. Andersen, in *Electrons at the Fermi Surface*, edited by M. Springford (Cambridge University Press, Cambridge, England, 1980).
[4] M. van Schilfgaarde and W. A. Harrison, Phys. Rev. Lett. **71**, 3870 (1993).
[5] D. D. Koelling, Phys. Rev. B **50**, 273 (1994).
[6] J. Unguris, R. J. Celotta, and D. T. Pierce, Phys. Rev. Lett. **67**, 140 (1991).
[7] S. Mirbt, H. L. Skriver, M. Alden, and B. Johansson, Solid State Commun. **88**, 331 (1993).
[8] P. M. Levy, J. L. Fry, and E. C. Ethridge, in *Magnetic Thin Films, Multilayers and Surfaces*, edited by S. S. P. Parkin (Materials Research Society, Pittsburgh, 1991), p. 189.
[9] H. L. Skriver and N. M. Rosengaard, Phys. Rev. B **43**, 9538 (1991).
[10] O. K. Andersen, Phys. Rev. B **12**, 3060 (1975); H. L. Skriver, *The LMTO Method* (Springer-Verlag, Berlin, 1984).
[11] O. K. Andersen, O. Jepsen, and D. Glötzel, in *Highlights of Condensed-Matter Theory*, edited by F. Bassani, F. Fumi, and M. P. Tosi (North-Holland, New York, 1985); O. K. Andersen, Z. Pawlowska, and O. Jepsen, Phys. Rev. B **34**, 5253 (1986).
[12] S. H. Vosko, L. Wilk, and M. Nusair, Can. J. Phys. **58**, 1200 (1980).
[13] J. Kudrnovsky, P. Weinberger, and V. Drchal, Phys. Rev. B **44**, 6410 (1991).
[14] S. L. Cunningham, Phys. Rev. B **10**, 4988 (1983).
[15] E. Fawcett, Rev. Mod. Phys. **60**, 209 (1988).
[16] P. Bruno and C. Chappert, Phys. Rev. B **46**, 261 (1992).
[17] M. D. Stiles, Phys. Rev. B **48**, 7238 (1993).
[18] M. van Schilfgaarde and F. Herman, Phys. Rev. Lett. **71**, 1923 (1993).
[19] K. Schwartzman, J. L. Fry, and Y. Z. Zhao, Phys. Rev. B **40**, 454 (1989).
[20] S. Mirbt, O. Ericsson, B. Johansson, and H. L. Skriver, Phys. Rev. B **52**, 15 070 (1995).
[21] M. A. Rudermann and C. Kittel, Phys. Rev. **96**, 99 (1954).
[22] J. Mathon, M. Villeret, and D. M. Edwards, J. Phys. Condens. Matter **4**, 9873 (1992).
[23] C. G. Windsor, J. Phys. F **2**, 742 (1972).
[24] S. Mirbt, A. M. N. Niklasson, H. L. Skriver, and B. Johansson, J. Magn. Magn. Mater. **148**, 209 (1995).
[25] Z. Q. Qui, J. Pearson, and S. D. Bader, J. Appl. Phys. **73**, 5765 (1993); Z. Q. Qui, J. Pearson, A. Berger, and S. D. Bader, Phys. Rev. Lett. **68**, 1398 (1992).
[26] K. B. Hathaway and J. R. Cullen, J. Magn. Magn. Mater. **104-107**, 1840 (1992).
[27] P. H. Dederichs, in *Magnetismus von Festkörpern und Grenzflächen* (Forschungszentrum, Jülich, 1993).